A wind tunnel for the calibration of Mars wind sensors

C. F. Wilson* (1), A. L. Camilletti (1), S. B. Calcutt (1), P. M. Ligrani (2)

(1) Dept of Physics, Oxford University

(2) Dept of Engineering Science, Oxford University

Abstract:

A major limitation in the development of wind sensors for use on Mars is the lack of suitable testing and calibration facilities. A low density wind tunnel has been developed at Oxford University for calibration of wind sensors for Mars landers, capable of providing stable or dynamically varying winds, of air or carbon dioxide, at Martian pressures (5 – 10 mbar) and speeds (0.5 – 30 m/s), and temperatures of 200 – 300 K. The flow field in the test section was calculated using analytical and computational modelling techniques, and validated experimentally using a pitot probe. This facility's stability and accuracy offer significant advantages with respect to previous calibration facilities.

Keywords: Mars; Martian meteorological sensors; Wind tunnel; laminar flow; anemometer; calibration

* Corresponding author

1 Introduction

1.1 Science Rationale

Measuring the near-surface winds on Mars is critical for a number of reasons. Near-surface winds represent a boundary condition for the rest of the atmospheric circulation; it is at the surface that most of the heat input to the atmosphere occurs; it is here that sources and sinks of volatiles like water and methane occur; and, particularly, near-surface winds determine the surface-atmosphere exchanges of dust, governing the onset and subsidence of dust storms. Near-surface winds are also critical from an engineering point of view for future exploration programmes, both for safe landing and for continued operation of landers and/or aerobots.

Measurement of wind on Mars is difficult, due largely to the low density of the atmosphere. Many different techniques of wind measurement on Mars have been proposed, including dynamic pressure devices like 'windsocks' (Sullivan et al., 2000) and telltales (Gunnlaugsson et al., 2006), to ion drift devices (Evlanov et al., 2001), laser-based devices (Merrison et al., 2006), and ultrasonic devices (Dissly et al., 2005). All wind data from Mars to date, though, has come from thermal wind sensors on the Viking landers (Chamberlain et al., 1976) and the Mars Pathfinder lander (Seiff et al., 1997); thermal wind sensors are also baselined for the future Mars Science Laboratory (MSL) and ExoMars missions due to their simplicity of construction and robustness.

However, thermal wind sensors are sensitive to any change in thermal conditions, in particular to changes in air temperature. On Mars, during the daytime, the ground

rapidly warms up in the sun, setting up a strong temperature gradient in the lowest few metres of the atmosphere. This temperature inhomogeneity is then advected by atmospheric turbulence, leading to rapid and frequent temperature swings at a given location. This can be seen in the wind and temperature data from Viking Lander 2 shown in Figure 1. Data from Viking Lander 2 and Mars Pathfinder missions show that temperature swings of 10°C can occur over periods as short as 10 seconds. Because thermal wind sensors are particularly sensitive to swings in air temperature (as well as other thermal loads such as sunlight or inhomogeneity in thermal infrared loads), it is important that these can be replicated in test facilities. For example, calibrated wind data have still not been published for the Mars Pathfinder thermal wind sensor due to uncertainties in thermal conditions at the wind sensor. The development of this and other thermal wind sensors has been hampered by a lack of calibration facilities.

From the previous discussion, it is evident that there are no standard wind sensors available for use to calibrate test facilities. Laser-Doppler anemometry is currently used as a standard in some wind tunnels; however, this requires airborne particles in the flow, which is not always consistent with flight hardware cleanliness requirements. In this paper, we discuss different approaches which can be used to simulate Martian winds, highlighting the advantages and disadvantages of the different methods. We then describe in greater detail a wind tunnel developed specifically for the calibration of wind sensors for Mars.

1.2 Turbulent or laminar flow?

The first task in any wind tunnel design is to consider the Reynolds number of the flow – this characterizes the level of turbulence to be expected in the flow. The Reynolds number is given by $Re = uD\rho/\mu$, where u is flow velocity, D is a length (typically, the diameter of the wind tunnel test section), and ρ and μ represent respectively the density and dynamic viscosity of the fluid. In the rarefied Martian atmosphere, any wind tunnel with a diameter of order 1 m is likely to exhibit turbulent flow, because it will have a Reynolds number in excess of 10^4 for speeds above 10 m/s. This suggests the use of a wind tunnel < 0.5 m in diameter, in order to keep the Reynolds numbers below 10^4 and thus make it possible to achieve laminar flow.

In addition, the boundary layer at the wind tunnel walls is of greater thickness in a low density atmosphere than in the equivalent flow at higher density (the theoretical basis for this is discussed below in Section 2.1). Therefore, if the aim is to test in the central region of the flow, uninfluenced by boundary layers from either wall of the wind tunnel, it is useful to have a small length-to-width ratio. In summary, a large wind tunnel with a large length-to-width ratio will always exhibit large-eddy turbulence, especially at higher speeds.

Two leading Mars wind tunnels exhibit turbulent flow – the Danish Mars Wind Tunnel at Aarhus University, which is 0.4 m diameter x 1.5 m long (Merrison et al. 2002), and the Mars Wind Tunnel (MARSWIT) at NASA Ames Research Centre (e.g. White et al., 1997; Greeley et al., 2000), which is 1.3 m x 1.3 m in cross section and 13 m long. Turbulence in the wind tunnel is useful for studying dust transport

due to boundary layer turbulence, which is a particular focus for these two facilities, but not helpful for calibration of wind sensors. For this task it is preferable to have laminar flow in the wind tunnel, which is achieved by using a laminar flow nozzle, as will be explained below. As discussed above, the length of the wind tunnel must be kept relatively short in order to keep the boundary layer development to a minimum. This approach was used for calibration of the Viking Wind sensor (Henry & Greene, 1974), and is adopted again for the Oxford Mars wind tunnel.

1.3 Rotating arm, recirculating, or open-circuit wind tunnel?

Wind tunnels can be subdivided broadly into three categories, as shown in Figure 2; rotating arm, re-circulating, and open-circuit.

A rotating arm is perhaps the oldest form of wind testing facility, and is still used today thanks to its simplicity and low cost. A Mars wind sensor test facility at NASA's Jet Propulsion Laboratory (JPL) uses a rotating arm with a length of 1 m, rotating in a 3 m diameter chamber (D. Crisp, personal communication). Speeds obtainable in this facility are limited, for aerodynamic and mechanical reasons, to a maximum of 10 m/s, at which speed the arm is rotating at ~1.5 revolutions per second. Also, the centripetal acceleration inherent in rotating arm systems makes them unsuitable for use in calibrating mechanical wind sensors.

Another approach is to use a recirculating wind tunnel. In this case the entire system is contained within an environmental chamber, in which the required pressure and temperature are maintained; within this, one can construct a standard wind tunnel

using a fan and ducting to circulate the gas past the test piece. A Mars wind tunnel at the University of Aarhus in Denmark is of this type, and has a test section of 0.4 m diameter x 1.5 m long. This facility typically exhibits turbulent flow, which is well-suited to its primary focus on studies of dust and sand transport; this turbulence causes fluctuations in the wind speed quoted as ranging from 4% to around 16% (Merrison et al., 2006).

A disadvantage of all the re-circulating wind tunnels is that it is difficult to introduce sudden changes in either wind speed or temperature. One solution to this problem is to feed the test section with an external gas supply, with the flow speed governed by a high-pressure drop. Once it has passed through the test section, the gas is then evacuated using vacuum pumps. This again follows the approach used for Viking wind sensor calibration by Henry & Greene (1974), as mentioned above.

A hybrid approach is used by the MARS WInd Tunnel (MARSWIT), located at the NASA Ames Research Centre, which has a test section is 1.3 m W x 1.3 m H x 13 m in length (see e.g. Greeley et al., 2000). MARSWIT is an open-circuit wind tunnel located within a large (~4000 m^3) vacuum chamber. At Martian pressures, wind is generated by injecting high pressure air or CO_2 at the exit of wind tunnel such that suction is generated. This wind tunnel thus has the advantage of being capable of relatively rapid changes in velocity (thanks to the gas injection system), and yet has the advantages of stability in composition and temperature because it is located entirely within a large test chamber. Like the Danish Mars wind tunnel, MARSWIT has a high length-to-width ratio, in order to let the turbulent boundary layer develop. This is ideal for surface boundary layer and Aeolian studies, but make it ill-suited to calibration of wind sensors (see for example Seiff et al., 1997).

2 Oxford Mars wind tunnel: design

An open-circuit wind tunnel has been created, as is shown in Figures 3 and 4, and is called the Mars Environment Wind Tunnel. The present wind tunnel is an adaptation of a previously existing facility, the Low Density Wind Tunnel (LDWT), at the Southwell Laboratory of Oxford University's Department of Engineering Science. The LDWT already operated as an open-circuit wind tunnel of the type described above, so it was possible to use without modification the large vacuum chamber itself and its powerful vacuum pumping system. The flow conditions required for this work (cool subsonic gas at a few millibars) are very different from those of the original LDWT (heated hypersonic gas at a few microbars), so several new sub-systems had to be implemented. The designs of the different subsystems of the wind tunnel are described below.

2.1 Nozzle design

The optimum diameter of the wind tunnel's test section was obtained by dividing the maximum possible pumping speed, conservatively estimated at ~ 0.84 $m^3 s^{-1}$, by the maximum flow speed needed (30 m/s). This gives a test section area of ~ 0.03 m^2, corresponding to a test section of diameter D = 0.18 m. For carbon dioxide at pressures of 6 – 10 mbar and temperatures of 200 – 300 K, the gas density ranges from 3 to 9 g m^{-3}. Thus we can calculate that the Reynolds numbers of the flow will range from 80 to 10000. At lower Reynolds numbers the flow will clearly be laminar;

150 however, a well-designed nozzle is required in the range $10^3 < Re_D < 10^4$ to ensure
151 uniform and laminar flow in the test section.

152 When gas enters the vacuum chamber, it is travelling at near-sonic velocity in a
153 small-bore pipe, and is very turbulent. It first enters a settling chamber, where the gas
154 decelerates, and its pressure equilibrates at near-Martian pressure. A deflector plate is
155 put at the entrance to this chamber in order to facilitate deceleration and mixing of
156 the gas. The gas then passes through a series of screens. The first screen is a porous
157 sintered plastic plate (pore size 100 μm; thickness 3.2mm); this ensures an even
158 distribution of airflow across the cross-section of the wind tunnel. Parallel flow is
159 ensured by passing the flow through a honeycomb flow straightener (5 mm cell width
160 x 50 mm length), and then any residual vortices are broken into smaller cells by a
161 final wire mesh with 1 mm spacing. At this point the diameter of the flow is still 400
162 mm, greater than the 180 mm test section diameter. This larger diameter ensures that
163 the flow is still slow when the flow passes through the flow straightener and mesh,
164 which ensures that turbulent eddies can be quickly dissipated, resulting in laminar
165 flow even at the highest test speeds. Finally, a contracting nozzle is used to reduce
166 the flow diameter from 400 mm to 180 mm, accelerating the flow smoothly by a
167 factor of ~5. The test section, i.e. the location in the wind tunnel where the wind
168 sensor is placed, is simply at the outlet of the nozzle. A nozzle with a circular section
169 was used in preference to a rectangular one because it does not have corners, which
170 can introduce inhomogeneity into the flow.

171 The shape of the nozzle itself was based on established nozzle design principles; the
172 rate of change of the nozzle's cross section is rapid at first, then less so as the fluid is
173 accelerated (e.g. Barlow, 1999). The length of the nozzle is kept fairly short, so that

the boundary layer thickness is still small when the flow reaches the test section. The nozzle shape was chosen following finite-element modelling (FEM) calculations using a commercial Computational Fluid Dynamics (CFD) package (Fluent). The mesh used for the FEM calculation was a two-dimensional (axisymmetric) model, with a higher density of nodes in the boundary layer. The mesh used had 40 x 40 nodes; it was found that higher node densities did not significantly change the results (mesh densities of up to 120 x 60 elements were tried, which changed local flow velocities by less than 0.2%). A uniform inlet velocity was specified as a boundary condition. The output parameter of most interest is the radial profile of axial velocity at the test section, i.e. at the exit of the nozzle.

Flow profiles were calculated for various flow speeds ranging from 0.1 m/s to 20 m/s. These flow profiles are presented in Figure 5 as a proportion of u_{ave}, where u_{ave} is the averaged flow speed in the section ($u_{ave} = \int_0^R u(r) 2\pi r dr$). These calculations assumed that the test gas was carbon dioxide at p = 6 mbar and T = 250 K. At all speeds above 1 m/s, the variation in velocity across the central 45 mm of the test section is under 1%; at all speeds above 3.5 m/s, the variation in velocity across the central 45 mm of the test section is under 0.5%.

In order to validate and to understand better the FEM results, the velocity profile was also studied analytically by calculating boundary layer development. The boundary layer at the wall of the wind tunnel is expected to be laminar in all flow conditions. If the Reynolds number is calculated using the length of the wall ($x \sim 0.45$ m), it stays well below 3×10^5 – commonly accepted as a guideline value for the onset of turbulence in this case – for all test conditions. The displacement thickness of the

boundary layer was calculated using the Thwaites method for boundary layer development in accelerating flow (see e.g. Young, 1989). This states that the boundary layer momentum thickness θ is given by

$$\theta^2 = 0.45\nu u^{-6}\int_0^x \left[u(x)\right]^5 dx\,,$$

where $u(x)$ is the free stream flow velocity as a function of x, the distance along the wall, and ν is the dynamic viscosity of the fluid ($\nu = \mu/\rho$). The value of the integral on the right is proportional to u^5. Therefore the boundary layer thickness scales as $\theta^2 \sim \nu/u$, i.e. $\theta \sim Re^{-1/2}$. Therefore the profile calculated for any given flow conditions should be the same as that for any other flow conditions with the same Reynolds number.

Given the displacement thickness and the free stream flow velocity, the expected velocity profile in the boundary layer can be obtained using a numerical solution to the Blasius equation, as shown for example in Fay and Sonwalkar (1991). It is assumed that the flow is uniform in the centre of the nozzle, as long as the boundary layer thickness is significantly less than the radius of the nozzle, an assumption which breaks down at low speeds. Calculated velocity profiles are in good agreement with FEM results at $u > 3$ m/s, as will be shown below.

At very low velocities ($Re_D \leq 300$, corresponding roughly to $u \leq 2$ m/s), the displacement thickness becomes significant in comparison to the radius of the wind tunnel. In this case the flow profile approaches Poiseuille flow, i.e. fully developed laminar pipe flow, which has a quadratic dependence on radius.

This primary nozzle, with its diameter of 0.18 m, is designed for flow speeds ranging from ~ 0.5 to 30 m/s. A second nozzle is also sometimes used, with a diameter of 0.12 m, which allows flow speeds of up to 65 m/s (due to its smaller cross-sectional area). A third possibility is to remove the nozzle entirely, which permits operation at 0.1 – 6 m/s. At such low flow speeds, flow will be laminar with or without the aerodynamic nozzle. This also allows a large test section (400 mm in diameter), and removes the problem of the growing boundary layer which causes uncertainty in the exact flow speed at the test piece. A similar approach (a porous plug without a contoured nozzle) was used for low speed flow in the temporary Viking wind sensor test facility at NASA's Langley Research Centre (Henry & Greene, 1974).

In summary, the wind tunnel may be used with either a nozzle of 180 mm diameter, or with a smaller nozzle of 120 mm which allows higher flow speeds. The nozzles have been designed to produce laminar flow, in order to minimise spatial and temporal velocity non-uniformities in the test section, at speeds of up to 30 m/s (or up to 60 m/s for the 120 mm nozzle). The spatial non-uniformity in the central 2 cm of the flow field has been predicted, using finite-element modelling (FEM), to be less than 1% for all flow speeds above 1 m/s (or 2 m/s for the 120 mm nozzle).

2.2 Gas flow and pressure control

The wind tunnel can be run using either air or carbon dioxide. A large (~10 m^3) balloon, filled with CO_2 at room pressure, is used as the source reservoir. This system is used rather than using CO_2 directly from gas cylinders for two reasons. The main reason is that, at the high flow rates used in the wind tunnel, CO_2 would freeze the regulators in the flow path. This possibility is commonly avoided by heating the CO_2

241 immediately before it passes through the regulators, but this leaves one with warm
242 gas, the temperature of which would be dependent on the flow rate being used.

243 A single valve, immediately upstream of the pressure chamber, is used to set the
244 mass flow rate. All gas upstream of this flow control valve is at, or near, atmospheric
245 pressure; downstream of this valve, the gas is at or near Martian pressure (~6 mbar),
246 or in fact slightly higher due to pressure gradients along the short pipe connecting
247 this valve to the test chamber. In normal operation, then, this valve acts as a critical
248 orifice, such that the flow rate and upstream pressure are independent of the
249 downstream pressure, because the upstream-to-downstream pressure ratio at this
250 valve is less than 0.53 (Parkinson and Day, 1979). Using an ordinary rubber weir-
251 type vacuum valve for this purpose, it was found that the mass flow rate could be set
252 to a resolution of ~0.1% of the maximum flow rate (i.e. roughly 0.03 m/s), which is
253 more than adequate.

254 Once the mass flow through the wind tunnel is set, the chamber pressure is set by
255 using a valve immediately upstream of the vacuum pumps to provide an extra load on
256 the vacuum pumps by admitting air from the atmosphere (as shown at the right of
257 figure 3). Opening this valve increases the chamber pressure, and closing it decreases
258 the chamber pressure. This pressure control valve is controlled with a stepper motor
259 using a commercial proportional-integral-derivative (PID) controller, with adaptive
260 tuning. This works very well in practice, keeping the pressure constant to an accuracy
261 of ± 0.01 mbar without operator intervention. The PID loop has proved very effective
262 at dealing with sudden changes in load conditions, such as when the wind speed is
263 changed, typically regaining the equilibrium pressure within 10-20 seconds. The
264 pressure in the test chamber is measured using a capacitive transducer (MKS

265 Baratron, 0-10 torr range), whose calibration certificate shows it to have an accuracy
266 of 0.005 mbar.

267 2.3 Mass flow rate monitoring.

268 The primary measurement of the wind speed in the tunnel is obtained by measuring
269 the mass flow rate of gas entering the tunnel. This is constantly monitored by
270 measuring the pressure drop across an orifice plate, which is (to a first
271 approximation) proportional to the square of the flow rate. The flow rates in the wind
272 tunnel vary from ~ 0.1 to 10 g/s, so the differential pressure sensors must be capable
273 of accurately reading pressures varying over 4 orders of magnitude. Therefore two
274 orifice plates are used to cover the full range, respectively 6 mm and 14 mm in
275 diameter. The larger orifice is used for higher flow rates (mass flow > 3 g/s), and is
276 monitored using a single 0-100 mbar differential pressure sensor (SensorTechnics
277 HCXM series). The smaller orifice plate is monitored using two differential pressure
278 sensors, with ranges of 0-10 mbar and 0-100 mbar respectively. This leads to a
279 differential pressure measurement accuracy of <1% of the reading, across the whole
280 range of flow rates.

281 The flow rate is determined using British Standard (BS) 1042, Sections 1:1, 1:2, 1:4.
282 According to the BS, the absolute accuracy of this method of flow rate determination
283 is 1% to 2%. The absolute accuracy of the mass flow determination in the wind
284 tunnel is thus estimated at 2% to 3 %. The resolution of the system is better than this,
285 though – the repeatability of the differential pressure sensors is 0.25% of their full-
286 scale range (limited at present by the resolution of the analogue-to-digital converter

used to record their output). Thus the precision to which flow conditions can be repeated is better than 1% of flow speed, for all flow speeds above ~1 m/s.

Note that the orifice plates allow determination of the *total* mass flow rate into the wind tunnel; if one divides this by the fluid density and by the cross-sectional area of the wind tunnel one can calculate the *average* velocity in the wind tunnel, u_{ave}. The local flow velocity at any point in the test section is then deduced from the modelling results presented in Figure 5. However, these results should be verified using local flow speed measurements in the test section

2.4 Local flow speed measurements

In order to characterise the spatial and temporal variations of velocity in the test section of the wind tunnel, one needs a method of measuring local flow velocity. In several other Mars wind tunnels, local flow velocity is measured through laser-doppler anemometry (LDA), using dust particles suspended flow. Dust cannot be used in the Oxford facility because it would damage the vacuum pumps. In principle, LDA could be used with oil droplets or smoke particles, but this is not compatible with cleanliness requirements in the facility.

To characterise the flow profiles in the wind tunnel, we used a pitot tube mounted on a three-dimensional translation stage to enable it to be moved throughout the test section. This incorporates both static tappings (which face perpendicular to the flow direction, thus measuring the absolute ambient pressure), and a pitot probe (facing into the flow). The difference between the static and the pitot pressure is the dynamic pressure, equal to $p_{dyn} = ½\rho u^2$. The density ρ is well known because the chamber pressure and temperature are being measured, which means that the speed u can be

calculated on the basis of the dynamic pressure measurement. The density of the gas is accurately known (to better than 0.1%), so the pitot probe offers an absolute measurement of local flow velocity with which to calibrate the wind tunnel.

The dynamic pressure is extremely low in the Martian atmosphere, due to a combination of low density and low wind speeds (p_{dyn} < 10 Pa for all wind speeds below 30 m/s). The most sensitive differential pressure sensor commercially available (Furness Controls FCO-332) has a full-scale sensitivity of 20 Pa and an accuracy of 0.03 Pa. Therefore, an accuracy of 10% or above in wind speed measurement can only be obtained for wind speeds of 6 m/s and above, for CO_2 at 7 mbar and 250 K. This inability to use the pitot tube at low wind speeds emphasizes once again that the dynamic pressures associated with light winds on Mars are extremely small and difficult to measure.

Another important source of error when using the pitot probe in this wind tunnel is fluctuations in the static pressure of the chamber, i.e. the ambient pressure of the gas. These fluctuations are the result of the dynamic equilibrium between the pumping speed and the gas inlet speed. The pressure control system can hold the chamber pressure steady to within 1 Pa, i.e. 0.01 mbar, which is stable enough for most purposes of environmental simulation. However, these fluctuations in static pressure are large compared to the dynamic pressures of 0.3 – 10 Pa measured at the pitot tube; this is a problem because the dynamic pressure being measured is the difference between the static pressure and the total pressure in the pitot tube. To give an estimate of the importance of this error: a fluctuation of 0.1 Pa due to static pressure fluctuations gives rise to an error of 1.3 m/s if the flow speed is 5 m/s, and 0.2 m/s if the flow speed is 30 m/s (These errors have been calculated assuming CO_2 at p = 7

mbar and T = 250 K). This source of error can be minimised by averaging over several readings (over ~ 20 seconds); however, it does mean that the pitot probe cannot be used to characterise the temporal variability of the flow speed. The temporal variability was characterised using a hot-film probe, as will be discussed in the next section.

Two flow profiles obtained using the pitot probe are shown in Figure 6. These profiles are for air at T = 299 K and p = 10 mbar, for flow speeds of 6.1 and 32.1 m/s (nominal flow speed in the centre of the test section, as calculated analytically). Analytical and finite-element modelling (FEM) results are included as well as experimental results; it can be seen that all three are in good agreement. The flow enhancement in the centre of the test section at high speed of about 1 m/s, seen in Figure 6, is not seen in the FEM results. This was due to use of a porous deflector (see Figure 3), which allowed a jet of air through at the centre of the test section. This has since been corrected by using a non-porous deflector.

A two-dimensional velocity profile of the test section is shown in Figure 7, obtained by scanning the pitot probe through the test section on a motorised translation stage. It can be seen that the velocity is uniform to ~ 3% over the central region of the test section. It is emphasized though that this constraint of 3% on the uniformity of the velocity field is due to the sensitivity of the velocity measuring technique to chamber pressure fluctuations as discussed above (due to the number of data points taken in this scan, it was not possible to time-average many readings for each data point). Thus it is suspected that the real velocity non-uniformity across the central area of the test section is less than 3%, quite possibly less than 1% as predicted by the FEM results.

2.5 Temporal stability

The present wind tunnel has been designed to produce laminar flow even at high wind speeds. In this section of the paper we consider first the theoretical basis of this statement and then discuss experimental evidence for fluctuations in the flow speed.

Let us consider the flow when it passes through the final mesh upstream of the test section. The final mesh has a wire spacing of 1 mm, so this is the maximum eddy size which can be expected in the flow at this point. The flow here is travelling five times more slowly than in the test section, because it has not yet passed through the accelerating nozzle. Therefore the Reynolds number here reaches a maximum of 16 (calculated by assuming CO2 at 10 mbar and 200 K, at a flow speed of 6 m/s and using L = 1 mm representing the mesh spacing). At these low Reynolds numbers, the energy in these eddies quickly dissipates through viscous processes. In any case, this dimension of 1mm is smaller than any of the wind sensors under consideration for future use on Mars so are expected to be undetectable. However, in order to test this hypothesis we have looked for fluctuations in the flow speed experimentally.

As described above, the pitot tube could not be used to measure temporal variations of local flow velocity due to its sensitivity to static pressure fluctuations. In order to characterise temporal fluctuations in the local flow speed, then, we need to use a different technique. For this purpose we used a hot-film anemometry probe which was a flight spare wind sensor from the Viking Lander, kindly provided to us by Jim Tillman of the University of Washington. This consisted of a platinum film deposited onto the surface of a quartz cylinder, 0.5 mm in diameter x 10 mm long (Davey et al., VMIS design report, 1973). The Viking wind sensor electronics were not available,

381 so the sensor was driven using a commercial constant-temperature anemometry
382 (CTA) bridge (Dantec 55M10). We obtained a calibration curve to relate power
383 dissipation to wind speed. Because this calibration curve was obtained with respect to
384 the wind tunnel's measurement of wind speed, we can not use the Viking wind
385 sensor as an absolute calibration standard for the Oxford wind tunnel. However, the
386 calibration curve does permit us to quantify the magnitude of velocity fluctuations in
387 the wind tunnel.

388 Time series of velocity measurements, obtained with the hot film probe positioned in
389 the centre of the test section, are presented in Figure 8 for flow velocities of 6.7 and
390 25.4 m/s. The y error bars represent the sampling resolution limit of the analog-to-
391 digital converter used to record the data. (each reading represents the average of 100
392 readings taken over the interval of 200 μs; this was routinely performed on all ADC
393 channels to reduce electrical noise). It can be seen that, at frequencies of < 1 Hz, the
394 velocities appear stable to within 0.1%.

395 If there is any turbulence in the flow, though, it would be expected to be at higher
396 frequencies. When its output was measured with an oscilloscope, the thermal wind
397 sensor was found to be sensitive to turbulence at up to 5 kHz (this was found by
398 placing it in a turbulent boundary layer). However, no measurable fluctuations in
399 flow speed were found when the wind sensor was placed in the centre of the wind
400 tunnel's test section. Based on the sensitivities of the equipment used, this places an
401 upper bound of 1% on velocity fluctuations in the centre of the wind tunnel for
402 velocities over 5 m/s.

Another measure of temporal stability of the flow in the wind tunnel comes from the orifice plate flow meters. At high flow speeds, the flow rate at the orifice plates is occasionally observed to fluctuate by ~ 0.3%, perhaps due to turbulence at the flow control valve (this valve emits a 'whistle' which fluctuates slightly in pitch at high flow rates). This fluctuation is only large enough to be detectable at u > 20 m/s; at this speed the fluctuations are only ~± 0.06 m/s, i.e. ~± 0.3%. This is a very small fluctuation, and represents a significantly smaller fluctuation than would be encountered in turbulent wind tunnels (c.f. 4% to 16% quoted for the Aarhus wind tunnel (Merrison et al., 2006).

2.6 Temperature control

Gas entering the test section can be cooled by passing it through a heat exchanger immediately before it enters the wind tunnel. Cooling power is provided by a closed-cycle cascade cooler (PolyCold PFC1100), which is capable of delivering 1 kW of cooling power at -100°C. The temperature of the heat exchanger is controlled using another PID loop to switch the cooling circuit on and off. The minimum temperature at which the wind tunnel can be run is around 200 K; this is limited by heat losses from the nozzle assembly (these are reduced by covering it with an insulating blanket, not shown in Fig. 3). In future, it may be possible to run at temperatures down to 170-180 K by pre-cooling the reservoir and nozzle, although it will always be difficult to operate so close to the freezing temperature of carbon dioxide.

Although the gas stream itself is cooled, the test chamber itself remains at room temperature. This has two implications for testing. First of all, it means that one cannot simulate cold conditions with zero wind: as soon as the wind is turned off,

426 anything in the test section warms up, through a combination of radiative and
427 convective heat transfer. Secondly, it means that the thermal IR radiative background
428 on any object in the test section has a brightness temperature of ~293 K rather than
429 the 150 – 250 K which might be more appropriate for Mars. This second effect is
430 especially important to consider for thermal wind sensors. This thermal IR
431 background temperature could be controlled in future by incorporating a thermal
432 shroud with an independent cooling loop, which would allow independent control of
433 the effective thermal IR background temperature; however, this has not yet been
434 implemented.

435 The Oxford wind tunnel provides a different and complementary test environment
436 compared to other current Mars wind tunnels, such as the one at Aarhus University.
437 The most important difference is that the Oxford wind tunnel is designed to give
438 laminar rather than turbulent flow. The second important difference is that the
439 Oxford wind tunnel is open-circuit rather than closed-circuit. Re-circulating (closed-
440 circuit) wind tunnels offer a stable pressure and temperature environment; in contrast,
441 the temperature and pressure in the Oxford facility are a result of a dynamic
442 equilibrium. The disadvantage of this is that it is difficult to keep the temperature
443 stable with changes in flow speed and pressure. However, this dynamic balance
444 means that conditions can be changed very rapidly. Wind speed can be changed from
445 0 to 30 m/s (or vice versa) in < 1 second, which allows testing of the response times
446 of meteorological instrumentation. The chamber pressure, too, can be changed
447 quickly: For example, it takes ~10 seconds to change the set-point from 6 mbar to 7
448 mbar. Although such rapid pressure changes are not representative of conditions on
449 Mars, it does mean that one can rapidly cycle through a set of test conditions. The

450 temperature in the test section can also be rapidly varied because it too, as discussed
451 above, is a result of a dynamical equilibrium. If operating at a constant flow speed, it
452 takes several minutes to change the set temperature by, say, 10°C, because of the
453 thermal mass of the heat exchanger. However, a rapid temperature change (e.g. 10°C
454 in 10 seconds) can be obtained by altering the flow rate to change the thermal loads.
455 In conclusion, the dynamical balances of flow, pressure, and temperature in the open-
456 circuit Oxford Mars wind tunnel offer many opportunities for testing responses to
457 transients which are quite different, and complementary to, the stable environment of
458 a closed-circuit tunnel.

459 ### 2.7 Wind direction variation

460 Although the test section of the wind tunnel is only 0.18 m in diameter (or 0.12 m if
461 using the smaller nozzle), the test chamber is 1.5 m in diameter, allowing plenty of
462 space for ancillary equipment such as rotation or translation stages. The most
463 frequent piece of equipment used is a motorised rotation stage used to change the
464 effective wind direction at the wind sensor. The test area is also large enough to
465 allow 2-D rotational stages to be used, e.g. to measure sensitivity to pitch and yaw
466 angles.

467 ## 3 Conclusions

468 A wind tunnel optimised for testing of sensors in Martian pressures and wind speeds
469 has been designed and implemented. The wind tunnel provides laminar flow of air or
470 carbon dioxide at pressures of 5 – 10 mbar, temperatures of 200 – 300 K, and speeds
471 of 0.5 – 30 m/s (dependent on pressure and temperature selected). The nominal test

472 section is 180 mm diameter, although a second nozzle of 120 mm diameter can also
473 be used to attain higher speeds (up to ~ 60 m/s).

474 Detailed analytical and finite element modelling techniques have been used to
475 characterise the facility's flow characteristics. By measuring mass flow rate using a
476 set of orifice plates on the gas inlet, the Reynolds number of the flow in the test
477 section can be determined with an absolute accuracy of 2 to 3%. Experimental
478 confirmation of flow profile predictions were obtained using a pitot probe for speeds
479 of above ~ 5 m/s, and these show very good agreement with modelling predictions.
480 The absolute accuracy in flow speed of ±3%, and the stability of the flow to within
481 ±0.3%, compare favourably with that achieved in other Mars wind sensor calibration
482 facilities.

Bibliography

Barlow, J.B., 1999. Low-speed wind tunnel testing. Wiley, New York.

British Standard 1042, *Measurement of fluid flow in closed conduits*, Sections 1.1 (1981) and 1.4(1992). Also BS ISO TR 15377 (1998), BSI, London.

Chamberlain, T.E., Cole, H.L., Dutton, R.G., Greene, G.C., Tillman, J.E., 1976. Atmospheric measurements on Mars: the Viking meteorology experiment. Bulletin of the American Meteorological Society 57, 1094-1104.

Davey, R., Chamberlain, T., Harnett, L., 1973. Viking Meteorology Instrument Sensor Design analysis report. TRW Systems Group document no. METC-021 (code ident. 11982), unpublished.

Dissly, R.W., Banfield, D.J., Lasnik, J., Waters, J.T., McEwan, I.J., Richardson, M.I., 2005. Development of a Martian Sonic Anemometer. DPS meeting #37, abstract #18.05.

Evlanov, E.N., Zubkov, B.V., Nenarokov, D.F., Linkin, V.N., Zavjalov, M.A. & Tyuryukanov, P.M., 2001. Gas-Discharge Anemometer for the Investigation of Flow Dynamics in Rarefied Gas Media. Cosmic Research 39 (5), 484-490.

Fay, J.A. and Sonwalkar, N., 1991. Fluid Mechanics. MIT, Boston.

Greeley, R., Wilson, G., Coquilla, R., White, B., & Haberle, B., 2000, Windblown dust on Mars: laboratory simulations of flux as a function of surface roughness. Planetary and Space Science 48, (12-14), p 1349-1355

Gunnlaugsson, H.P., Akinlade, O., Gross, M.A., Jensen, S.K., Lange, C.F., Leer, K., Lemmon, M.T., Lyckegard, F., Madsen, M.B., Merrison, J., Nørnberg, P., Olsen, M., Shinohara, C., Smith, P., 2006. The Telltale Wind Experiment for the NASA Phoenix Mars Lander 2007. EGU general assembly 2006, abstract #06064.

505 Henry, R. M., Greene, G. C., 1974. Anemometers for Mars. In: Dowdell, R.B. (Ed.), Flow, its
506 measurement and control in science and industry. Instrument Society of America.

507 Merrison, J.P., Bertelsen, P, Frandsen, C., Gunnlaugsson, H.P., Knudsen, J.M., Lunt, S., Madsen,
508 M.B., Mossin, L.A., Nielsen, J., Nørnberg, P., Rasmussen, K.R., Uggerhøj, E., 2002. Simulation of the
509 Martian dust aerosol at low wind speeds. Journal of Geophysical Research, 107 (E12), 5133

510 Merrison, J.P., Gunnlaugsson, H.P., Kinch, K., Jacobsen, T.L., Jensen, A.E., Nornberg, P., Wahlgreen,
511 H., 2006. An integrated laser anemometer and dust accumulator for studying wind-induced dust
512 transport on Mars. Planetary and Space Science 54 (11), 1065-1072.

513 Parkinson, K.J., Day, W., 1979. The Use of Orifices to Control the Flow Rate of Gases. Journal of
514 Applied Ecology 16 (2), 623-632.

515 Seiff, A, Tillman, J.E., Murphy, J.R., Schofield, J.T., Crisp, D., Barnes, J.R., LaBaw, C., Mahoney, C.,
516 Mihalov, J.D., Wilson, G.R., and Haberle, R.M., 1997. The atmosphere structure and meteorology
517 instrument on the Mars Pathfinder lander. Journal of Geophysical Research 102 (E2), 4045-4056.

518 Sullivan, R., Greeley, R., Kraft, M., Wilson, G., Golombek, M, Herkenhoff, K, Murphy, J., Smith, P.,
519 2000. Results of the Imager for Mars Pathfinder windsock experiment. Journal of Geophysical
520 Research 105 (E10), 24547-24562.

521 White, B.R., Lacchia, B.M., Greeley, R., Leach, R.N., 1997. Aeolian behavior of dust in a simulated
522 Martian environment. Journal of Geophysical Research-Planets 102 (E11), 25629-25640.

523 Young, A. D., 1989. Boundary Layers 1st edition. BSP Professional Books.

Figure Captions

Figure 1 - A twenty-minute sequence of wind and temperature data measured by the Viking Lander 2. The sampling interval for the data shown is 1.2 seconds. (Data provided by Jim Murphy, NMSU).

Figure 2 – Three basic types of low density wind testing facility. In each diagram the grey square indicates the position of the wind sensor (or test piece), the thick black lines represent the walls of a vacuum chamber, and arrows represent airflow.

Figure 3 – Schematic diagram of wind tunnel

Figure 4 – Close-up of the test section of the wind tunnel, showing the nozzle and the translation stage used to move the pitot tube through the flow field. The test chamber is roughly 1.5 m diameter x 1.5 m in length.

Figure 5 – FEM calculations of flow profile in the 180 mm nozzle, calculated for carbon dioxide at $p = 6$ mbar and $T = 250$ K.. At all velocities above 1 m/s the velocity variation in the central section (defined as $r < 22.5$ mm) of the wind tunnel is < 1 %. At low velocities the solution approaches the quadratic profile of Poiseuille flow (fully-developed laminar pipe flow). Velocity at the centre of the test section is expressed as a proportion of u_{ave} ($u_{ave} = \int_0^R u(r) 2\pi r dr$).

Figure 6 – Velocity profiles in the wind tunnel. Analytical and FEM results are presented, as are experimental measurements obtained using the pitot probe. Profiles shown are average speeds of 6.1 and 32.1 m/s, in air at 10 mbar and T = 299 K; these flow profiles are equivalent to what is obtained in CO_2 at 250 K and 6 mbar at velocities of 3.8 and 19.7 m/s respectively

Figure 7 – 2D flow profile at test section, obtained using the pitot probe. The test gas was air at p_{test} = 5.5 mbar, T = 293 K.

Figure 8 – Time series of velocity measurements in the centre of the test section at two different velocities, in air at 7 mbar, obtained using a thermal wind sensor (see text for details).

Figure 1

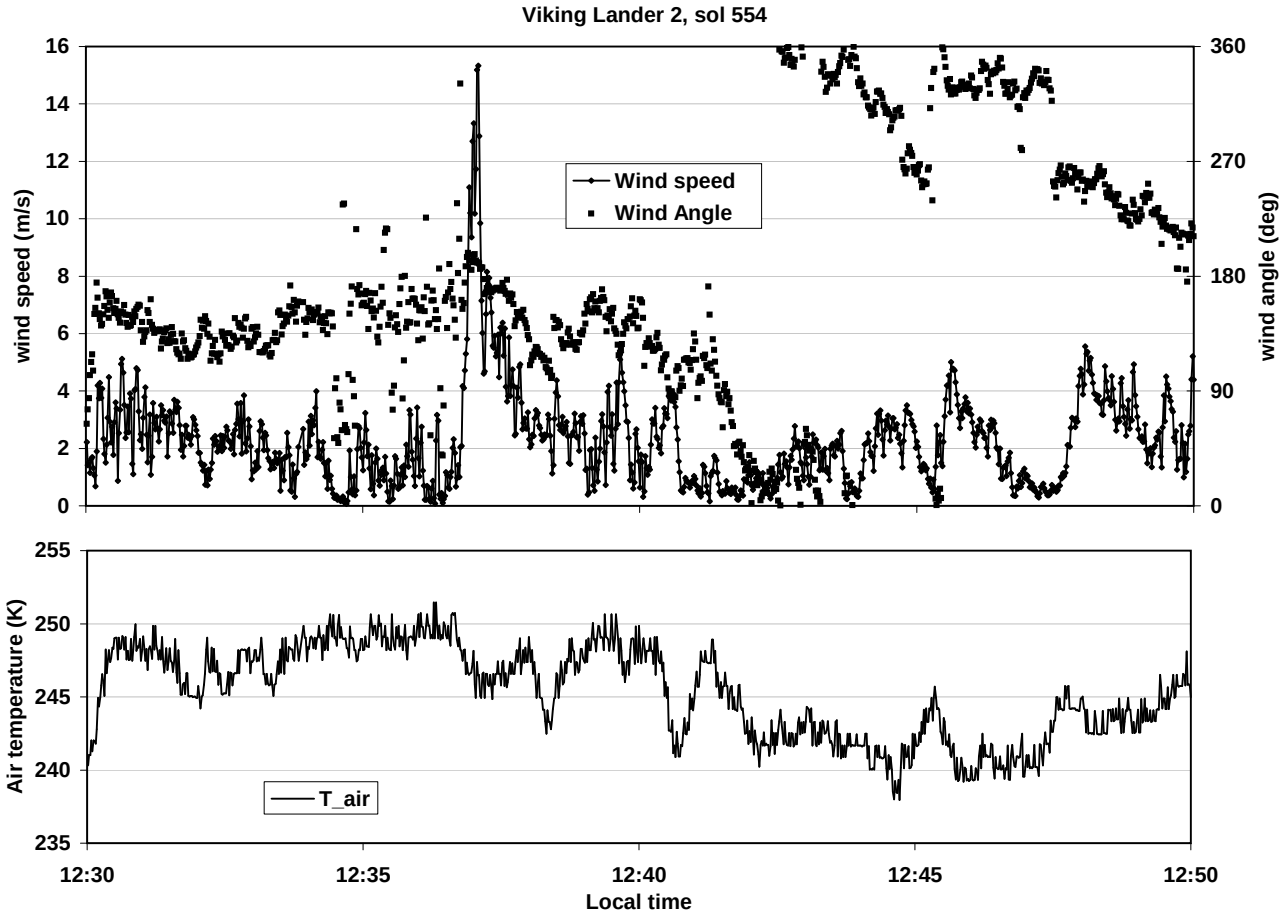
Viking Lander 2, sol 554
wind speed (m/s)
wind angle (deg)
Wind speed
Wind Angle
Air temperature (K)
T_air
Local time
12:30
12:35
12:40
12:45
12:50

Figure 2

a) rotating arm

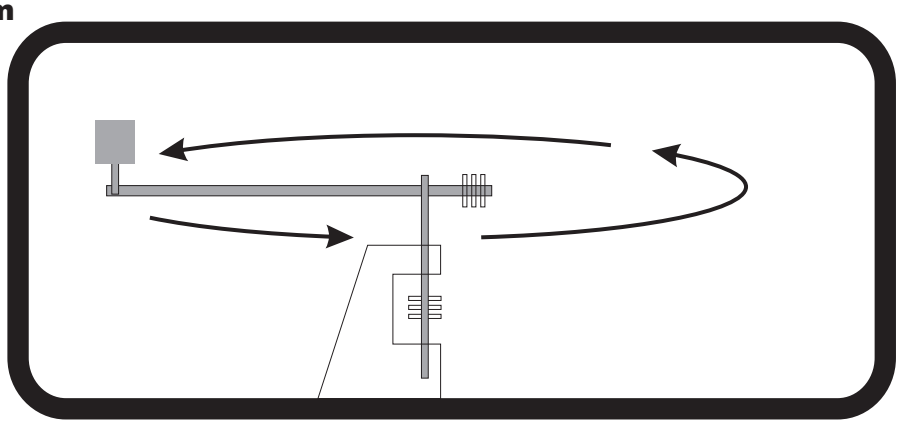

b) recirculating

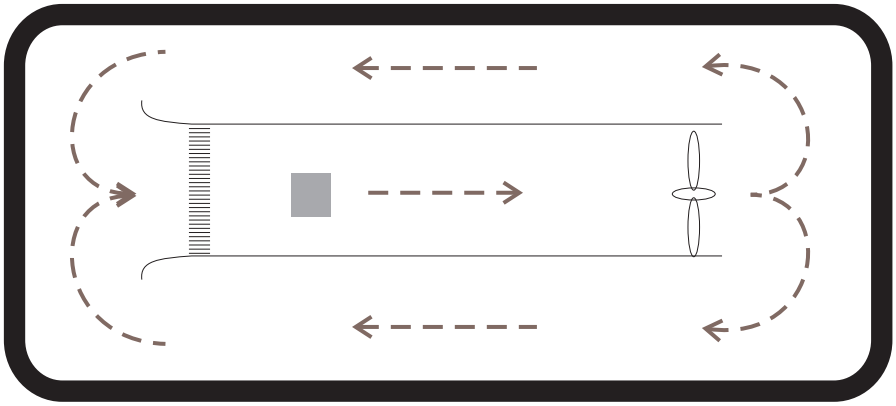

c) open-circuit

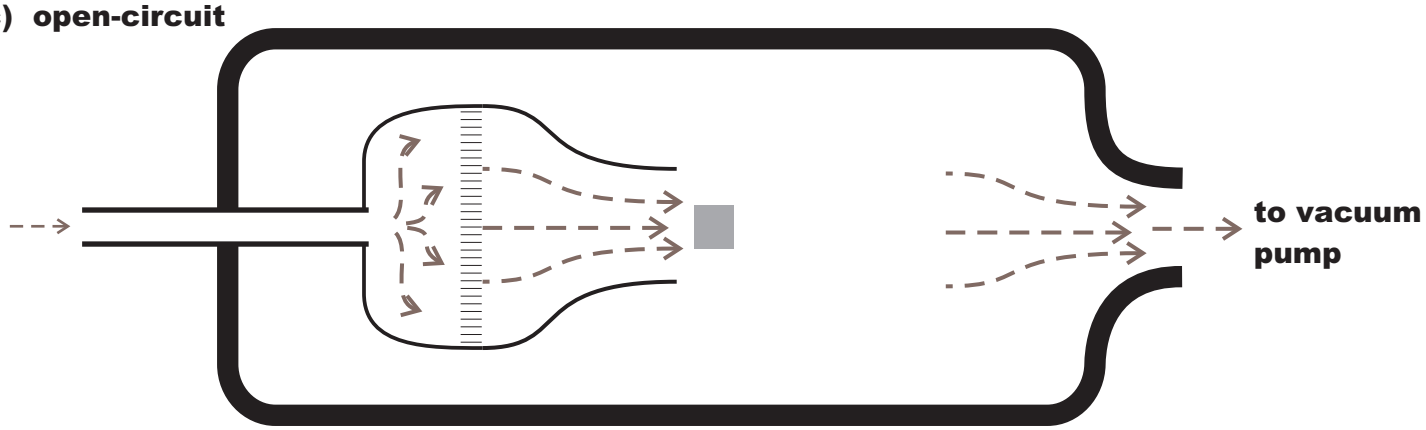

Figure 3

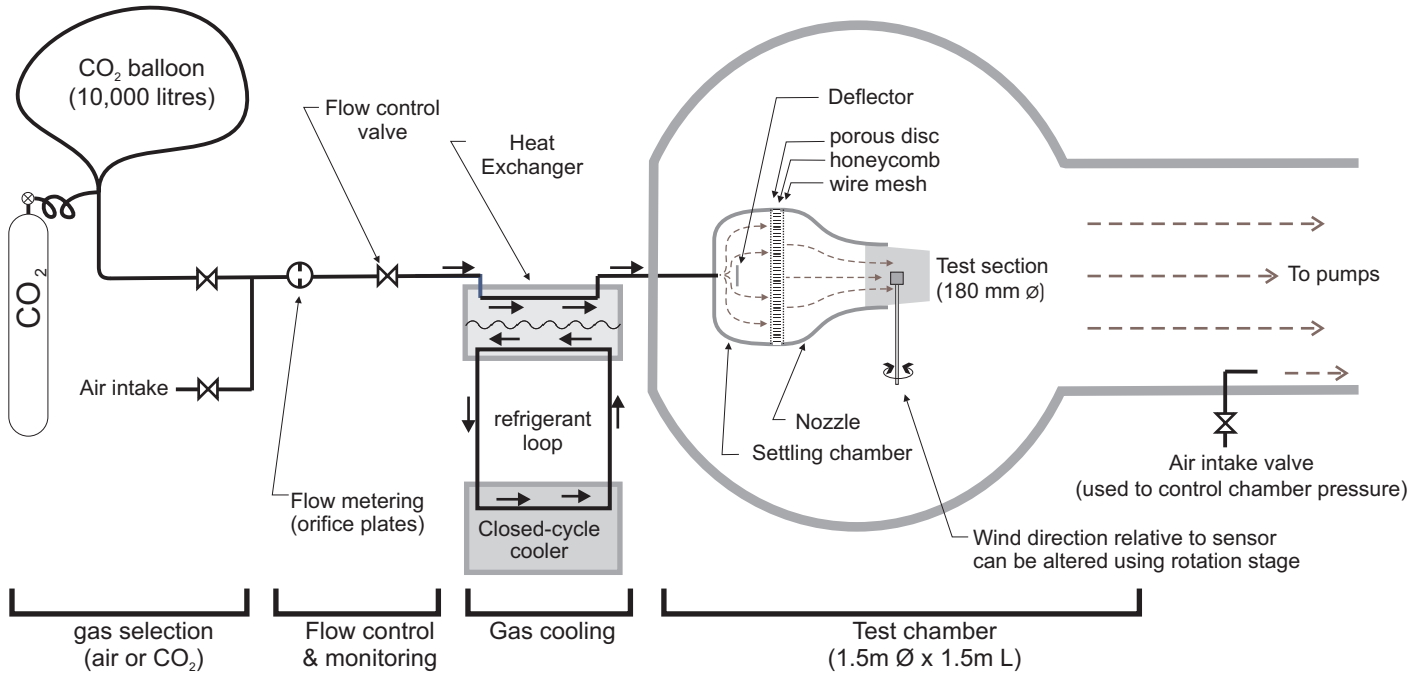
CO_2 balloon
(10,000 litres)
CO_2
Air intake
Flow control
valve
Heat
Exchanger
Flow metering
(orifice plates)
refrigerant
loop
Closed-cycle
cooler
Deflector
porous disc
honeycomb
wire mesh
Test section
(180 mm ø)
Nozzle
Settling chamber
To pumps
Air intake valve
(used to control chamber pressure)
Wind direction relative to sensor
can be altered using rotation stage
gas selection
(air or CO_2)
Flow control
& monitoring
Gas cooling
Test chamber
(1.5m Ø x 1.5m L)

FIGURE 4

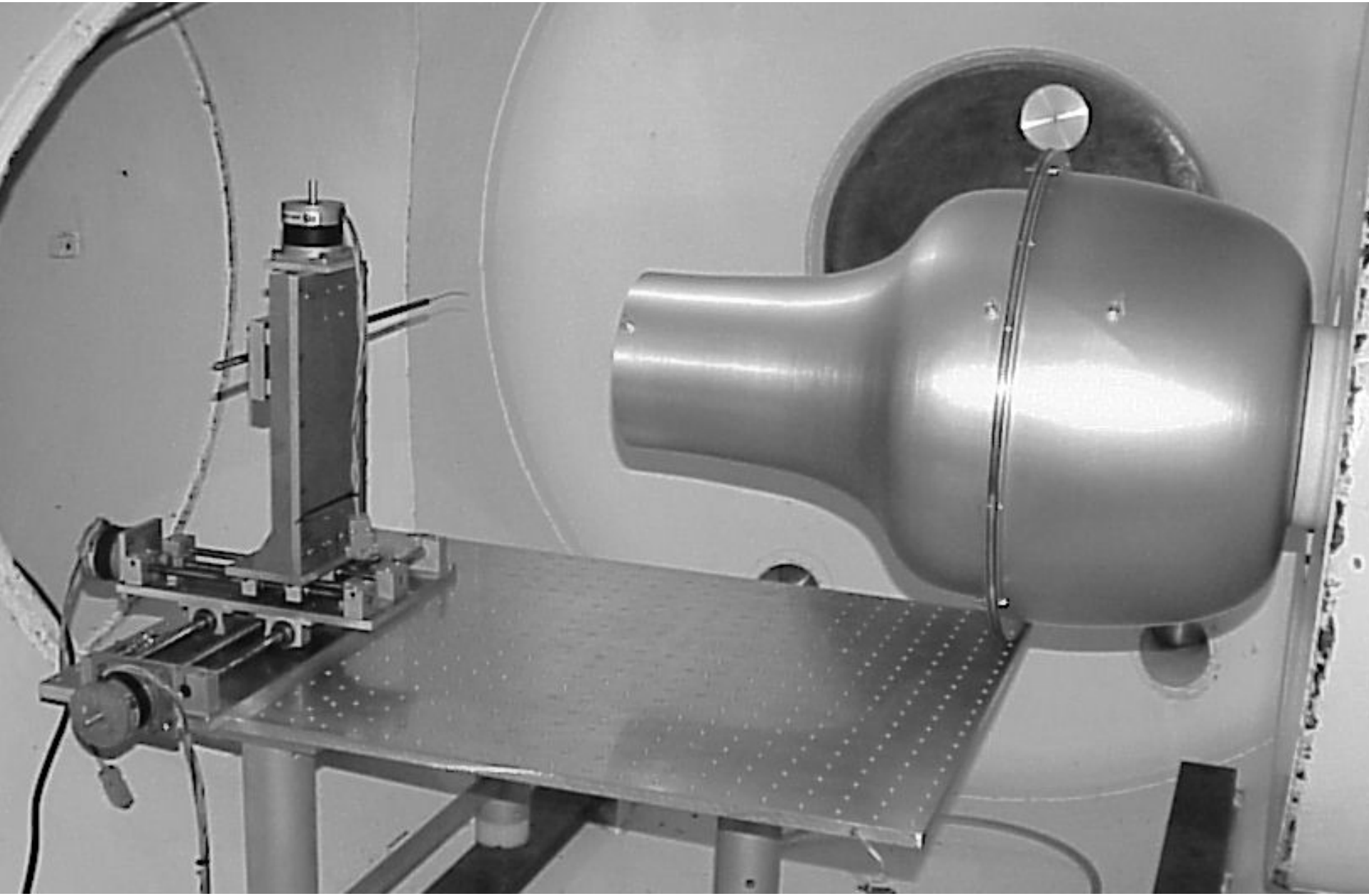

FIGURE 5

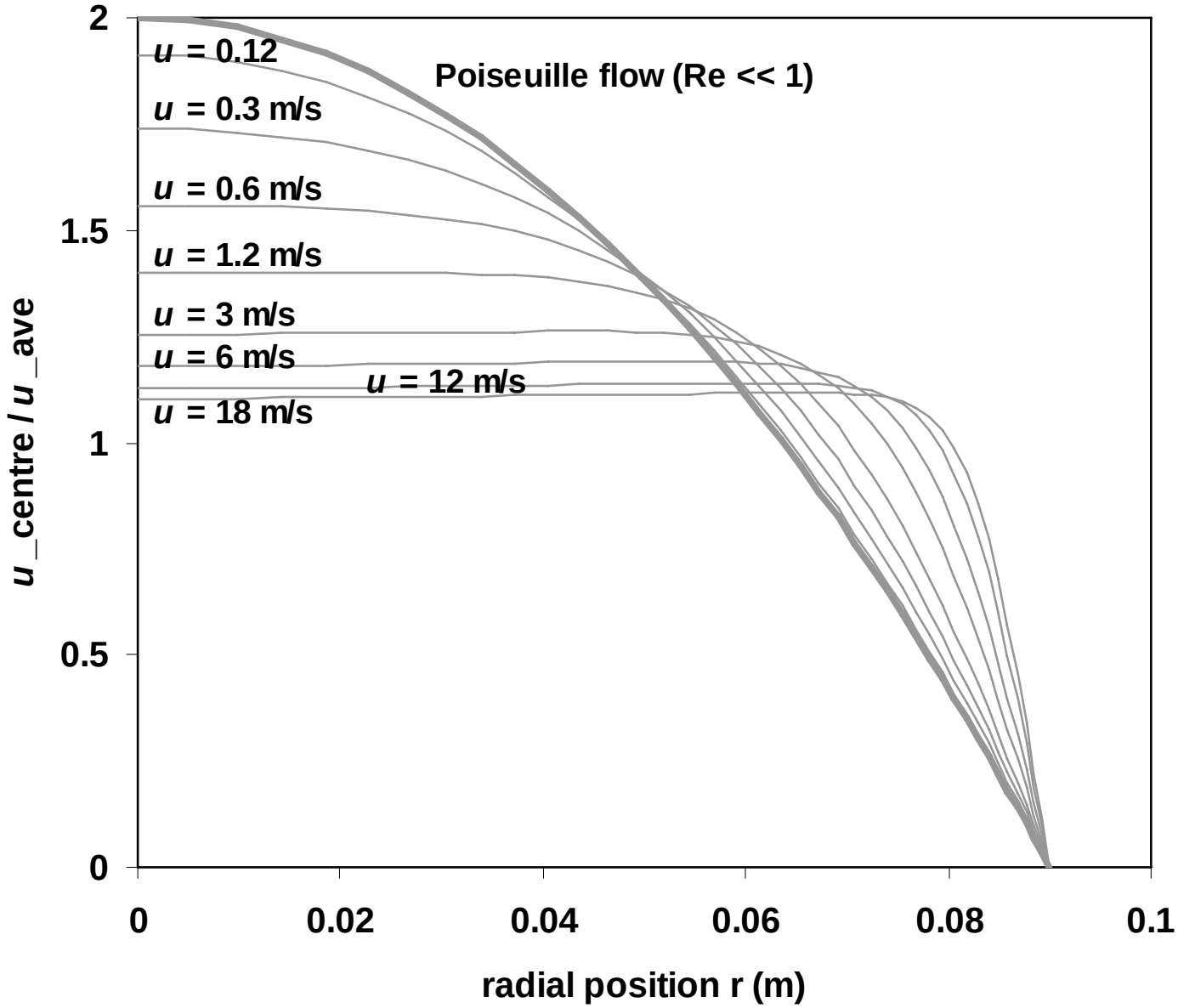
Poiseuille flow (Re << 1)
u = 0.12
u = 0.3 m/s
u = 0.6 m/s
u = 1.2 m/s
u = 3 m/s
u = 6 m/s
u = 12 m/s
u = 18 m/s
u_centre / u_ave
radial position r (m)
0
0.5
1
1.5
2
0
0.02
0.04
0.06
0.08
0.1

Figure 6

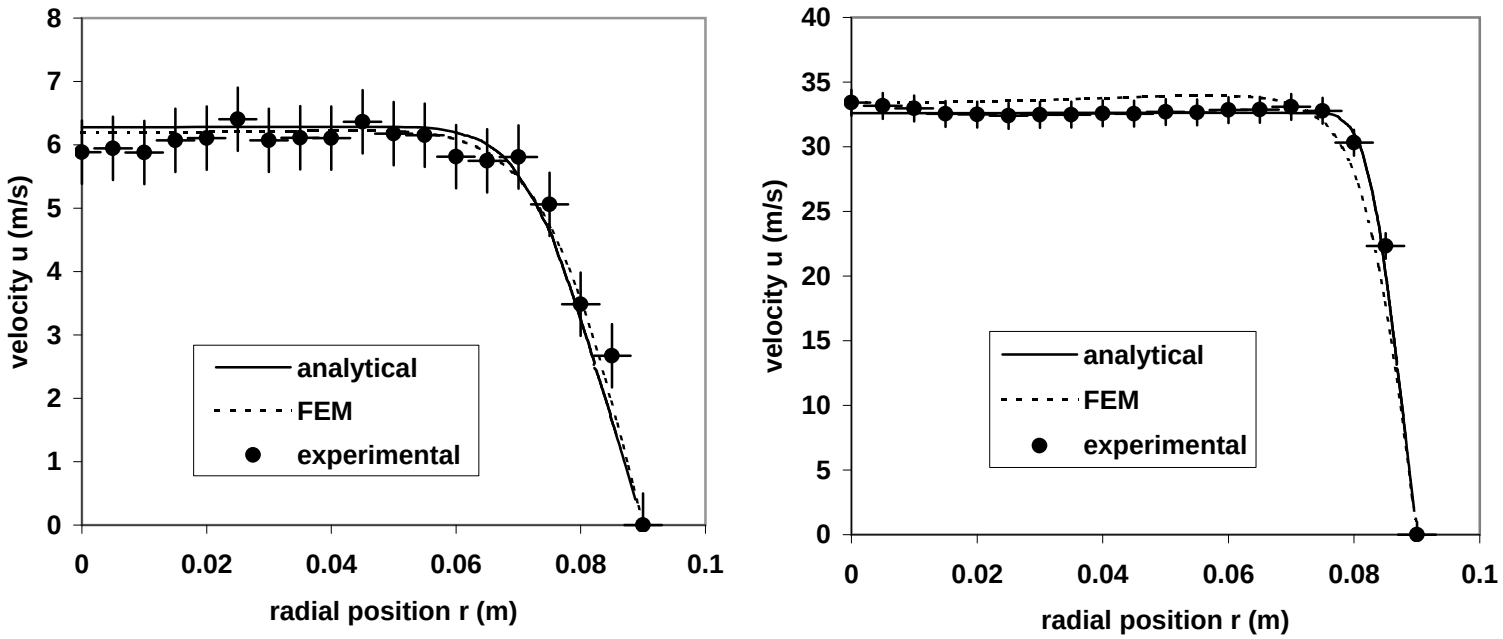
velocity u (m/s)
radial position r (m)
analytical
FEM
experimental
0
1
2
3
4
5
6
7
8
0.02
0.04
0.06
0.08
0.1
velocity u (m/s)
radial position r (m)
analytical
FEM
experimental
0
5
10
15
20
25
30
35
40
0.02
0.04
0.06
0.08
0.1

Figure 7
Click here to download high resolution image

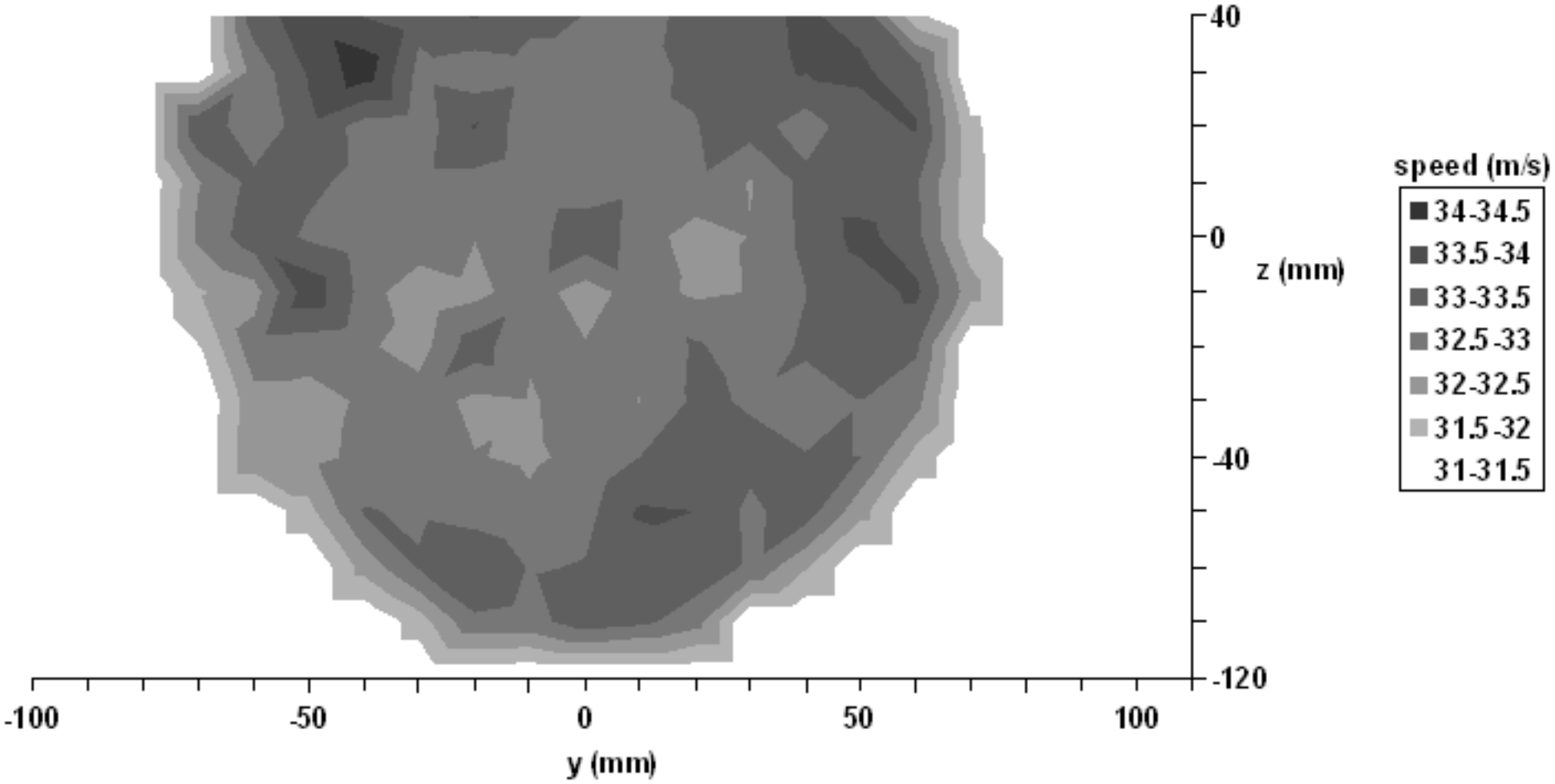

Figure 8

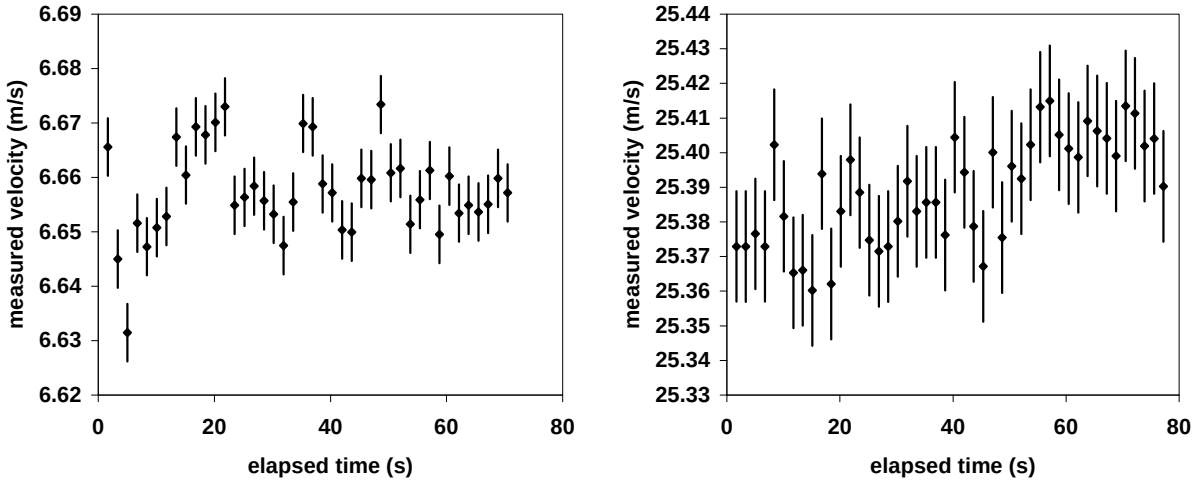
6.69
6.68
6.67
6.66
6.65
6.64
6.63
6.62
measured velocity (m/s)
0
20
40
60
80
elapsed time (s)
25.44
25.43
25.42
25.41
25.40
25.39
25.38
25.37
25.36
25.35
25.34
25.33
measured velocity (m/s)
0
20
40
60
80
elapsed time (s)